Article:
Staines, K.A., Javaheri, B., Hohenstein, P. et al. (7 more authors) (2017) Hypomorphic conditional deletion of E11/podoplanin reveals a pivotal role in osteocyte dendrite elongation. Journal of Cellular Physiology. ISSN 0021-9541

https://doi.org/10.1002/jcp.25999

ORIGINAL RESEARCH ARTICLE

Hypomorphic conditional deletion of E11/Podoplanin reveals a role in osteocyte dendrite elongation†

Running head: E11 is key in osteocyte dendrite elongation

Katherine A. Staines[1,2*], Behzad Javaheri[3], Peter Hohenstein[1], Robert Fleming[1], Ekele Ikpegbu[1,4], Erin Unger[1], Mark Hopkinson[3], David J. Buttle[5], Andrew A. Pitsillides[3], Colin Farquharson[1]

[1] Roslin Institute and R(D)SVS, The University of Edinburgh, Easter Bush, Midlothian, UK

[2] School of Applied Sciences, Edinburgh Napier University, Sighthill Campus, Edinburgh UK

[3] Comparative Biomedical Sciences, Royal Veterinary College, Royal College Street, London, UK

[4] Michael Okpara University of Agriculture, Nigeria

[5] Dept of Infection, Immunity and Cardiovascular Disease, University of Sheffield, Sheffield UK

*** Corresponding author:**

Katherine A. Staines

School of Applied Sciences, Edinburgh Napier University, Sighthill Campus, Edinburgh EH11 4BN

Email: k.staines@napier.ac.uk

Tel: 0131 455 3369

†This article has been accepted for publication and undergone full peer review but has not been through the copyediting, typesetting, pagination and proofreading process, which may lead to differences between this version and the Version of Record. Please cite this article as doi: [10.1002/jcp.25999]

Additional Supporting Information may be found in the online version of this article.

Received 3 April 2017; Revised 5 May 2017; Accepted 8 May 2017
Journal of Cellular Physiology

DOI 10.1002/jcp.25999

Abstract

The transmembrane glycoprotein E11/Podoplanin (Pdpn) has been implicated in the initial stages of osteocyte differentiation. However, its precise function and regulatory mechanisms are still unknown. Due to the known embryonic lethality induced by global Pdpn deletion, we have herein explored the effect of bone specific Pdpn knockdown on osteocyte form and function in the post-natal mouse. Extensive skeletal phenotyping of male and female 6-week-old Oc-cre;$Pdpn^{flox/flox}$ (cKO) mice and their $Pdpn^{flox/flox}$ controls (fl/fl) has revealed that Pdpn deletion significantly compromises tibial cortical bone microarchitecture in both sexes, albeit to different extents ($P<0.05$). Consistent with this, we observed an increase in stiffness in female cKO mice in comparison to fl/fl mice ($P<0.01$). Moreover, analysis of the osteocyte phenotype by phalloidin staining revealed a significant decrease in the dendrite volume ($P<0.001$) and length ($P<0.001$) in cKO mice in which deletion of Pdpn also modifies the bone anabolic loading response ($P<0.05$) in comparison to age-matched fl/fl mice. Together, these data confirm a regulatory role for Pdpn in osteocyte dendrite formation and as such, in the control of osteocyte function. As the osteocyte dendritic network is known to play vital roles in regulating bone modeling/remodelling, this highlights an essential role for Pdpn in bone homeostasis.

Keywords: Osteocytes; E11; osteocalcin; osteoblasts; dendrite

Contract grant sponsor: Arthritis Research UK & Biotechnology and Biological Sciences Research Council (BBSRC). **Contract grant number:** 20413 (ARUK) & BB/J004316/1 (BBSRC)

This article is protected by copyright. All rights reserved

Introduction

Osteocytes are the most numerous of all the cells within bone and are critical regulators of bone structure and function. Most original paradigms have proposed that osteocytes are passive in their formation (Skerry et al., 1989; Nefussi et al., 1991; Palumbo et al., 2004). Recent evidence, however, now indicates that initial 'embedding' involves their active contribution with vital transcriptional and dramatic morphological transformations (Holmbeck et al., 2005). Osteocytes have a highly specialized morphology with numerous dendritic processes extending from their cell body, connecting them with other osteocytes and with cells lining the bone surfaces, creating a large syncytium to enable cell-cell communications. Osteocytes play an integral role in maintaining bone homeostasis by regulating bone modeling and remodeling through their production of the Wnt inhibitor sclerostin, and through communicating with bone-resorbing osteoclasts by RANKL production (Balemans et al., 2001; Xiong et al., 2011; Nakashima et al., 2011; Dallas et al., 2013).

Although it is well recognized that osteocytes are derived from osteoblasts, the mechanisms which govern this transition (osteocytogenesis) are yet to be fully elucidated. Several different genes have been implicated in influencing osteocytogenesis, one of which encodes for E11/Podoplanin (Pdpn) (Zhang et al., 2006). Pdpn is a mucin-like, transmembrane glycoprotein, which undergoes O-glycosylation leading to the production of different glycoforms. Pdpn is up-regulated by hypoxia in the lung (Cao et al., 2003); IL-3 and PROX-1 in the lymphatic system (Hong et al., 2002; Groger et al., 2004) and by TGF-β in fibrosarcoma cells (Suzuki et al., 2005).

Few studies have investigated the precise function of Pdpn in osteocytes. We have previously shown that Pdpn is expressed by early embedding osteocytes, thus identifying it as a factor which likely contributes to the vital, early stages of osteocyte differentiation (Staines et al., 2016a). It is known that Pdpn expression in osteocytes is up-regulated in response to mechanical strain in vivo (Zhang et al., 2006) and that increased Pdpn expression, through overexpression in ROS 17/2.6 cells and through stabilization by proteasome inhibitors in MLO-A5 cells, leads to the formation of long dendritic processes (Sprague et al. 1996; Staines et al., 2016a). The formation of these cytoplasmic processes is abrogated in cells pre-treated with siRNA targeted against Pdpn (Zhang et al., 2006). Although these data support an important role for Pdpn in

dendritic process formation, a key feature of the differentiating osteocyte, the underpinning mechanisms remain to be fully defined.

Whilst in vitro studies are informative, to fully disclose the biological function of Pdpn during in vivo osteocytogenesis and bone modeling/remodeling, it is essential to study an in vivo model of Pdpn deletion to enable a thorough examination of its functional role. Global deletion of Pdpn is perinatal lethal due to the essential role of Pdpn in lung and epithelial cell function (Zhang et al., 2006). We have therefore generated a Pdpn conditional knockout mouse to examine how deletion of Pdpn influences osteocytogenesis and the skeletal phenotype of these mice. We have used the well-characterized osteocalcin (OC)-cre promotor mouse (Zhang et al., 2002) as the expression of osteocalcin by late osteoblasts ensures that we eliminate Pdpn expression from late osteoblasts as they transition to the osteocyte phenotype. Using an osteocyte-specific cre mouse would have invalidated our experimental approach as it would have precluded our ability to study the role of Pdpn in osteocyte formation; osteoblasts would already have undergone differentiation into osteocytes. It is also pertinent to add that an osteocyte specific cre-promotor mouse does not currently exist. Here we show that a significant reduction in the expression of Pdpn in mice affects tibial microarchitecture, compromises osteocyte dendrite elongation and thereby implicating Pdpn as a regulator of both osteocyte form and function.

Results

Oc-cre mediated bone-specific deletion of Pdpn

The genotypes from the breeding strategy were born at the expected Mendelian frequency, and all cKO mice exhibited survival indistinguishable from that of fl/fl control mice. To confirm that the Pdpn floxed allele was selectively deleted in bone in cKO mice, we performed PCR analysis using primers designed to specifically detect Pdpn alleles before (Tm1c) and after (Tm1d) cre-recombination. As expected, the Tm1d allele was only present in the cKO mice revealing selective deletion of Pdpn in bone (Fig. 1B). The presence of reduced levels of the retained Tm1c allele in the bones from cKO mice indicates that complete Pdpn deletion was, however, not achieved (Fig. 1B). This bone-selective hypomorphic expression of Pdpn in cKO mice was confirmed by immunohistochemical and immunoblotting data. In both genotypes, immunolabelling for Pdpn showed extensive expression throughout all soft tissues including the lung, kidney and liver (Fig. 1C). Pdpn immunolabelling was also

observed in the growth plate chondrocytes of all mice (Fig. 1C). Osteoblasts in both the fl/fl and the cKO mice also stained positively for Pdpn. In the trabecular and cortical bone of the fl/fl mice, osteocytes and their dendritic processes exhibited positive immunolabelling for Pdpn (Fig. 1D). However, in the cKO mice, approximately 70% of osteocytes did not label positively for Pdpn, thereby indicating a significant reduction in bone Pdpn in these cKO mice ($P<0.001$; Fig. 1D & E). Similarly, western blotting revealed little Pdpn expression in the bones from cKO compared to fl/fl mice (Fig. 1F). Together these data confirm the hypomorphic loss of Pdpn expression selectively from bone in our cKO mice.

Bone-selective ablation of Pdpn has no effect on the gross skeletal phenotype

Analysis of total body weight (g) of male or female 6-week old mice showed no significant differences between genotypes (male fl/fl – 20.4 ± 0.5; male cKO – 19.1 ± 0.4; female fl/fl – 16.3 ± 0.6; female cKO – 16.2 ± 0.5; n>4/genotype/sex). Similarly, no differences were observed in the tibia lengths (mm) in cKO and fl/fl mice (male fl/fl – 16.2 ± 0.1; male cKO – 16.1 ± 0.2; female fl/fl – 15.6 ± 0.2; female cKO – 15.5 ± 0.1; n>4/genotype/sex). Whole mount skeletal staining of mice also revealed no obvious gross differences in Alcian blue or Alizarin Red staining between cKO and fl/fl mice (Fig. 1G & H). Gait parameters of freely moving mice using the CatWalk gait analysis system were also unchanged (Suppl. Fig 1). Together these data suggest that the bone-selective deletion of Pdpn has no effect on the gross skeletal phenotype of mice.

Pdpn deletion significantly alters tibial cortical bone microarchitecture

Assessment of cortical bone mass by µCT (CSA/mean cortical thickness) revealed that Pdpn deletion produces statistically significant alterations in tibial cortical mass and shape, to differing extents, in both male and female cKO compared to fl/fl control mice. Specifically, CSA is unaffected in female cKO mice but is significantly lower in male cKO compared with male fl/fl mice at ~40-65% of tibial length ($P<0.05$; Fig. 2A). In addition, mean cross sectional thickness was significantly lower at several regions in male cKO compared to male fl/fl mice ($P<0.05$), however, Pdpn deletion resulted in an increase in mean cross sectional thickness at several regions along the tibial length in female cKO compared with fl/fl control mice ($P<0.05$; Fig. 2B). Together these data indicate that the conditional deletion of Pdpn produces a deficit in the cortical tibial microarchitecture in both male and female mice, with a greater

effect observed in the male mice. Despite this, no significant differences were observed in the trabecular bone volume/tissue volume (BV/TV), trabecular number (Tb.N), trabecular thickness (Tb.th), trabecular separation (Tb.Sp), or trabecular pattern factor (Tb.Pf) in male or female cKO mice in comparison to age-matched fl/fl control mice (Table 1).

Hypomorphic deletion of Pdpn results in gender-dependent effects on tibial structural parameters

To provide an estimate of tibial resistance to bending forces, we calculated second moment of area around minor (I_{min}) and major axes (I_{max}) (Fig. 3A & B). This showed a reduction in I_{min} along the tibia length in female cKO compared to female fl/fl which was most pronounced in midshaft and distal tibia ($P<0.05$, Fig. 3A). Statically significant reduction in I_{min} was also apparent in the tibia of male cKO compared with their male fl/fl controls, less so at the midshaft but more proximally ($P<0.05$, Fig. 3A). Overall, the trend in cKO mice was for smooth lowering of I_{min} proximodistally, which contrasts markedly from fluctuations in I_{min} along the tibia length of age-matched fl/fl control mice. For I_{max}, the trend was similar for female cKO and their fl/fl controls ($P<0.05$, Fig. 3B), however, the effect in male cKO seemed to be more proximal and midshaft ($P<0.05$, Fig. 3B). Tibial ellipticity and resistance to torsion (J) was mostly affected in female cKO compared with female fl/fl ($P<0.05$, Fig. 3C & D) with only small regions affected in male cKO compared with their male controls ($P<0.05$, Fig. 3C & D). This suggests that tibiae in female cKO are weaker than in fl/fl control mice. Indeed our 3-point bending data shows a 52% increase in stiffness in the female cKO in comparison to fl/fl mice ($P<0.01$; Table 2). No other significant differences were observed in bone strength, work to rupture or maximum load between genotypes in either gender (Table 2).

Bone selective Pdpn hypomorphism does not affect osteocyte differentiation but causes disruption of the osteocyte dendritic network

To examine how Pdpn deletion affects osteocytogenesis, we examined the mineralization and differentiation potential of cultured primary calvaria osteoblasts from Pdpn cKO and fl/fl mice. Alizarin red staining (Fig. 4A) and subsequent quantification (Fig. 4B) revealed no significant differences in the mineralization capabaility of Pdpn cKO primary osteoblasts in comparison to fl/fl mice. Consistent with this, we observed no significant differences in the gene expression of the

osteocyte markers Sost and Phex in our Pdpn cKO cells at days 0, 7, 14 and 21 of culture (Fig. 4C & D). Similarly, no significant differences in Dmp1 expression were observed at days 0, 7 and 14 although at day 21 of culture, there was a small significant decrease in the expression of Dmp1 in our Pdpn cKO cultures ($P<0.05$; Fig. 4E). Taken together, these data suggest that the bone selective hypomorphic deletion of Pdpn does not influence osteocyte differentiation.

Due to the proposed role for Pdpn in osteocyte dendrite formation and elongation, we sought to determine whether Pdpn deletion modifies osteocyte organisation by measuring 3D morphometric parameters in high resolution images obtained from nano-CT at the tibia–fibula junction. Our morphometric evaluation of the cortical bone microarchitecture at the tibia–fibula junction shows that Pdpn deletion does not affect numbers of osteocyte lacunae (N.Lc/Ct.TV; Table 3) or lacunar volume (Lc.V/Ct.TV; Table 3). Interestingly, no significant effect on vascular porosity; canal number (N.Ca; Table 3), density (N.Ca/Ct.TV; Table 3) and volume (normalised by cortical tissue volume; Ca.V/Ct.TV; Table 3) was also evident in cKO bones.

Due to the reported function of the osteocyte in regulating bone remodeling and phosphate homeostasis, we next sought to examine whether our cKO mice exhibit differential expression of the osteocyte factor sclerostin, as well as serum phosphate. We observed no apparent differences in the expression of sclerostin in our cKO mice in comparison to fl/fl mice (Fig. 4F). Similarly, our assessment of osteoclast and osteoblast numbers by TRAP and H&E staining, respectively and found no significant differences in their number between cKO and fl/fl mice (Fig. 4G & H). Serum phosphate levels were also similar in cKO and fl/fl mice (Fig. 4I). The osteocyte and its canalicular-lacunar organisation also have another pivotal role in the bone's adaptive response to mechanical stimuli. We therefore next sought to examine whether tibiae deficient in Pdpn exhibit a modified response to mechanical loading. As expected, and in line with previous data, fl/fl mice show a significant load-induced increase in cortical bone cross-sectional thickness at the proximal diaphysis region of the tibia ($P<0.01$, Fig. 5A - C). Although the scale of the load-induced increase was statistically smaller than in fl/fl mice ($P<0.05$), cKO mice also exhibited a significant increase in the tibial cross-sectional thickness in response to loading ($P<0.05$, Fig. 5A - C; compared to contralateral control). As expected, in both our fl/fl and cKO mice, a decrease in sclerostin immunolabelling was observed in cortical bone osteocytes of the loaded limb in comparison to osteocytes of the unloaded contralateral limb (Fig.

5D). There were however no differences in osteocyte sclersotin expression between loaded bones from fl/fl and cKO mice (Fig. 5D).

In the light of the relatively normal osteocyte organisation in cKO mice as disclosed by nano-CT (Table 3), the difference in response of cKO and fl/fl control mice to mechanical loading was somewhat surprising. Therefore, to determine whether this deficit in load-related bone adaptation was associated with any specific change in osteocyte morphology we next performed phalloidin staining of F-actin in fl/fl and cKO cortical bone. Subsequent 3D rendering (Fig. 5E) and quantitative analysis of osteocytes in the diaphyseal cortical bone confirmed our nano-CT data and revealed no significant differences in the total number of osteocyte cell bodies (Fig. 5F), the osteocytes cell body volume (Fig. 5G) or the osteocyte cell body sphericity (Fig. 5H) in cKO bone in comparison to age-matched fl/fl bone. Similarly, no significant differences were observed in the number of dendrites formed (Fig. 5I). However, a significant decrease in the mean dendrite volume (Fig. 5J, $P<0.001$) and the dendrite lengths (Fig. 5K, $P<0.001$) was noted in cKO in comparison to fl/fl mice, suggestive of a role for Pdpn in attainment of fully developed dendrites.

Discussion

We, and others, have previously shown that Pdpn promotes osteocytogenesis and dendrite formation in vitro (Zhang et al., 2006; Staines et al., 2016a). Our studies, described herein, have for the first time successfully generated a bone-specific conditional Pdpn hypomorphic mouse and we have confirmed a role for Pdpn in the attainment of fully elongated osteocyte dendrites.

Previous attempts to decipher the in vivo role of Pdpn in osteocytogenesis have involved global deletion of Pdpn in mice. In the lung, Pdpn is known as T1alpha or RT140 and it is expressed on the apical surface of the lung epithelial cells (Dobbs et al., 1988; Rishi et al., 1995). In mice, global deletion of this gene results in death at birth due to respiratory failure. This is associated with the failure of type II alveolar lung cells to differentiate into type I cells and as such, the lungs of these mice are unable to inflate as normal (Ramirez et al., 2003). T1alpha deletion in mice also produces lymphatic defects with pronounced lymphedema resulting in swelling of the limbs at birth (Schacht et al., 2003). A previous comprehensive study has attempted to analyze the effect of Pdpn deletion on the skeleton by generating a global Pdpn knock-out mouse by targeting exon 1 (Zhang et al., 2006). Whilst these mice did not

express Pdpn in bone, the animals died soon after birth from suspected lung defect. Although the authors were unable to study the effects of Pdpn deletion on the postnatal skeleton they were able to make some important observations. The general appearance of the embryonic Pdpn null and wild-type mice was similar. More specifically, they found no significant differences in the length or diameter of the femur, or in the femur cortical thickness. They did report an increase in the body weight of the Pdpn null mice, however this was attributed to lymphedema resulting from limb swelling (Zhang et al., 2006).

By using the cre-LoxP system targeted to exon 3 of the Pdpn gene, we have generated bone specific conditional knockdown mice which exhibited survival indistinguishable from that of fl/fl control mice. This has for the first time allowed us to study the role of Pdpn in bone development in the post-natal mouse. The normal survival rates of cKO mice contrasts with perinatal lethality of global $Pdpn^{-/-}$ mice (Zhang et al., 2006). Here we used the well characterized osteocalcin-driven cre promotor to drive Pdpn deletion. Oc-cre expression has previously been reported to be exclusive to late osteoblasts, with onset of expression just before birth and continuing throughout the mature osteoblast lineage (Zhang et al., 2002). This has therefore allowed us to examine the structure and function of the postnatal skeleton in the presence of reduced Pdpn expression in bone, where we observed significant differences in tibial cortical bone microarchitecture and in the volume and length of osteocyte dendrites likely leading to downstream effects on the tibia's anabolic response to loading.

Osteocytes play a vital role in regulating bone remodeling and their vast dendritic network is critical to cell-cell communication, maintaining cell viability and allowing the transfer of nutrients and waste products (Dallas et al., 2013). Accumulating evidence has suggested that Pdpn may play a critical role in dendrite formation; in MLO-Y4 cells, the deletion of Pdpn with siRNAs abrogated dendrite formation (Zhang et al., 2006). Conversely, the ectopic overexpression of Pdpn in keratinocytes induces plasma membrane extensions (Scholl et al., 1999), and in endothelial cells, the reorganisation of the actin cytoskeleton and the formation of long tube like structures (Schacht et al., 2003). Similarly, we have previously shown that stabilisation of Pdpn protein, through inhibition of endogenous proteasome activity, promotes dendrite formation through the RhoA/ROCK/ERM pathway (Staines et al., 2016a). RhoA is a small GTPase and a master regulator of various cellular processes

such as cytokinetics, cytoskeletal regulation, and cell migration (Takai et al., 2001). Pdpn is able to co-localise with the ezrin, radixin and moesin (ERM) family of proteins which are essential for the linkage of the actin cytoskeleton to the plasma membrane (Scholl et al., 1999; Martin-Villar et al., 2006; Martin-Villar et al., 2014). Our present data suggests that Pdpn deletion does not affect osteocyte differentiation and instead, strongly support a role for Pdpn in the formation of full length dendritic processes. Despite this, we did not observe any differences in the expression of factors involved in the osteocytic regulation of bone remodeling and phosphate homeostasis. Normal sclerostin expression in osteocytes within bone of Pdpn cKO mice is consistent with a lack of change in osteocyte number, shape and size in these mice. It is possible that the hypomorphic deletion of Pdpn expression in osteocytes does not affect the osteocyte's ability to regulate bone remodeling. Rather, the decreased magnitude of bone accrual in response to mechanical loading is likely a consequence of inadequate dendrite formation and a lack of critical osteocyte mechanoregulatory function.

Mechanosensation and mechanotransduction were the earliest functions ascribed to the osteocyte and since then, there has been a wealth of evidence defining their role and in particular, the role of the dendritic network in sensing mechanical loads. In recent years, the complex biochemical pathways through which the osteocyte converts its mechanical strain signals into a biological output have been unravelled. These include intracellular calcium, nitric oxide, ATP and prostaglandins and these have direct effects on osteoblasts to alter the bone microarchitecture (Dallas et al., 2013). On this basis, we therefore speculate that the restricted osteocytic dendrite network observed in our hypomorphic Pdpn cKO mice would likely lead to altered bone geometry and microarchitecture; the reduced dendritic network impairs the ability of the osteocyte to sense load and convert this to a biological signal affecting osteoblast function. It would obviously therefore be of interest to examine the expression of the aforementioned biochemical pathways in our Pdpn cKO mice in response to loading. Moreover, as the bone mechanical properties, including stiffness, depend upon the geometry of the bone shaft, it is likely that the reduction of the osteocyte dendritic network affects the mechanical properties as a secondary effect through these changes in the microarchitecture (Saffar et al., 2009).

Here we used whole bone µCT analysis to fully define these changes in microarchitecture and determine the estimated strength and rigidity of the bone through the study of the bone's cross sectional geometry. CSA is directly related to a bone's strength against compressive forces applied equally throughout the bone; factors such as bone shape and the effects of muscle contraction however result in long bones experiencing bending and torsional forces (Javaheri et al., 2015). We measured indices of rigidity, including maximum and minimum resistance against bending forces in the cross section, second moment of area around minor axis (I_{min}) and second moment of area around major axis (I_{max}) in male and female cKO tibia and their age-matched control mouse tibia. Our data, using this approach, revealed sex-dependent differences in cortical bone microarchitecture and in our estimation of tibial resistance to bending forces in cKO mice in comparison to control mice. These differences suggest that bone responses to dysfunctional osteocyte form and function may be sex-dependent. Similarly the differences in the regional responses in both male and female bones suggests that Pdpn may play differential roles in bone development and function. Interestingly, Bonewald and colleagues found osteocyte Pdpn expression was increased in an ulna loading model, but that this increase was not consistent along the length of the diaphysis (Zhang et al., 2006). This regional requirement for Pdpn function during physiological loading in the post-natal mouse may explain the differences noted in structural parameters of the Pdpn cKO mouse and in the relatively minor, albeit significant, reductions in load-related increases in cortical thickness in the bones of these mice.

Despite these changes in bone microarchitecture and osteocyte form in our Pdpn cKO mice our data reveals no effect of Pdpn deletion on the gross phenotype. This suggests that whilst Pdpn plays a role in dendrite length and bone microarchitecture, there may be redundancy associated with the function of Pdpn. Possible candidates include Dentin matrix protein 1 (DMP1). DMP1 is an acidic phosphorylated extracellular matrix protein that is part of the Small; Integrin-Binding LIgand, N-linked Glycoprotein (SIBLING) family along with bone sialoprotein (BSP), osteopontin (OPN), dentin sialophosphoprotein (DSPP) and matrix extracellular phosphoglycoprotein (MEPE). All of these family members contain an RGD sequence for integrin binding and can bind to hydroxyapatite (Staines et al., 2012). DMP1 is highly expressed by osteocytes and is restricted to the dendritic processes.

Deletion of DMP1 in mice causes remarkable defects in both tooth and bone (Ye et al., 2004; Ye et al., 2005). DMP1 knockout mice also display an abnormal lacuna-canalicular system, with a reduction in the number of canaliculi and a 2-fold expanded osteocyte lacunae with rough, not smooth, lacunar walls (Lu et al., 2011). The authors of this elegant study also showed that this phenotype can be rescued by the re-expression of the 57-kDa C-terminal fragment of DMP1 (Lu et al., 2011). DMP1 has been demonstrated to bind to the hyaluronan receptor CD44, a membrane bound protein thought to interact with the ERM family of proteins that are involved in actin cytoskeleton rearrangement and as such, the formation of the osteocyte dendritic processes (Jain et al., 2002).

As we did not achieve complete cre-recombination and consequently not a complete knock-out of Pdpn expression (~70% reduction) it is also possible that a low level of Pdpn expression is sufficient to drive osteocytogenesis. A more complete knock-out of Pdpn expression may be required to reduce dendrite formation to a level where bone function is pathologically compromised. Our decision to use the osteocalcin-cre promotor mouse to drive deletion of Pdpn selectively in bone was based on the onset of OCN expression. Despite this, there have been previous reports of incomplete recombination when using these mice (Xiao et al., 2010). As such it might be prudent to attempt another cre driver mouse. Such examples would include the col 2.3 kb (Col 2.3-Cre) and 3.6 kb (Col 3.6-Cre) fragments of the rat Col1a1 promoter or the osterix-cre mouse (Liu et al., 2004; Rodda et al., 2006).

In summary, our data confirm a role for Pdpn in the formation of full length dendritic processes during osteocytogenesis and suggest that dysfunctional osteocyte dendrite formation is sufficient to alter the bone microarchitecture. The generation of a viable post-natal bone specific Pdpn cKO will enable future research into understanding the importance of Pdpn in osteocyte function, and in particular to the in vivo effects of dysfunctional osteocyte formation on bone homeostasis.

Materials and methods

Generation of a Pdpn conditional knockout mouse

We obtained floxed Pdpn mice from the EUCOMM/KOMP, MRC Harwell, Oxfordshire UK and OC-cre mice as a kind gift from Thomas Clemens at John Hopkins Medicine, Baltimore, USA (Zhang et al., 2002). Pdpn floxed mice were

designed with the loxP sites around exon 3 (Fig. 1A). Mice were crossed to generate Oc-Cre;Pdpn$^{flox/flox}$ conditional knockout mice (cKO) as well as appropriate Pdpn$^{flox/flox}$ control mice (fl/fl). PCR based genotyping was performed on mouse DNA using a duplex PCR reaction for Cre (F: GCA TTA CCG GTC GAT GCA ACG AGT GAT GAG; R: GAG TGA ACG AAC CTG GTC GAA ATC AGT GCG) and Fabpi200 (F: TGG ACA GGA CTG GAC CTC TGC TTT CCT AGA; R: TAG AGC TTT GCC ACA TCA CAG GTC ATT CAG) and for Pdpn (F: TCC CAC ACC AGG TTT TGT GT; R: CAG TGA GCC ATC TCT CCA GC). Mice were kept in polypropylene cages, with light/dark 12-h cycles, at 21 ± 2°C, and fed ad libitum with maintenance diet (Special Diet Services, Witham, UK). All experimental protocols were approved by Roslin Institute's Animal Users Committee and the animals were maintained in accordance with UK Home Office guidelines for the care and use of laboratory animals. All analysis and data acquisition were completed on 6-week-old mice and tissue obtained from them.

Determination of Cre-mediated Recombination Efficiency

To determine the specificity and efficiency of Cre-mediated recombination, PCR analysis was performed on genomic DNA extracted from bones using a Qiagen DNA extraction kit according to the manufacturer's instructions. Primers were specific for alleles before recombination (Tm1c; F: TGG AAT GGC TGT GAG TTC TG; R: CTA AAA TGG AGT TGG AGA TGG ATA C) and after recombination (Tm1d; F: TGA GCG AGC AGA GGT CCT AA; R: GCG TCT GGC ACT CTC AGA AG).

Primary osteoblast isolation and culture

Primary calvarial osteoblasts were obtained from 3-day-old Pdpn cKO and fl/fl mice by sequential enzyme digestion of excised calvarial bones using a four-step process as has previously been described (Staines et al., 2013) [1 mg/ml collagenase type II in Hanks' balanced salt solution (HBSS) for 10 min; 1 mg/ml collagenase type II in HBSS for 30 min; 4 mM EDTA for 10 min; 1 mg/ml collagenase type II in HBSS for 30 min]. The first digest was discarded and the cells were re-suspended in growth medium consisting of a-MEM (Invitrogen, Paisley UK) supplemented with 10% (v/v) FCS (Invitrogen) and 1% gentamycin (Invitrogen). Osteoblasts were seeded at a density of 1×10^4 cells/cm^2 and cultured for up to 21 days with the addition of 2.5 mM β-glycerophosphate and 50 μg/ml ascorbic acid. At days 0, 7, 14 and 21,

Cells were either processed for RNA extraction or fixed in 4% paraformaldehyde and stained with 2% alizarin red (pH 4.2) for 5 min at room temperature. Alizarin red-stained cultures were extracted with 10% cetylpyridinium chloride for 10 min and optical density was measured at 570nm.

Gait analysis

Gait parameters of freely moving male mice were measured using the CatWalk gait analysis system (Noldus Information Technology, The Netherlands) as described previously (Masocha et al., 2009; Hammers et al., 2001). Each mouse was placed individually in the CatWalk walkway and allowed to walk freely and traverse from one side to the other of the walkway glass plate. Mice were habituated every day for two weeks prior to the test run, in which the gait of all mice was recorded three times and analysed using the CatWalk system. Analysis of the recording generated a wide range of parameters; those analysed are detailed in Supplementary Table 1.

In vivo loading

12-week old male mice were isoflurane-anaesthetised and the right tibia loaded as described previously using a well-established model for comparing architectural load-induced changes in tibiae in control and mutant mice in which the contralateral left tibia is used as control (De Souza et al., 2005). Briefly, axial compressive loads were applied by a servo-hydraulic materials testing machine (Bose, UK) via custom-made cups which hold knee and ankle joints flexed and the tibia vertically. The loading pattern consisted of a trapezoidal wave, with peak 11N loads for the cKO and 12N for the WT mice for 0.05 s, rise and fall times 0.025 s each and baseline hold time of 9.9 s at 2 N (calibrated for peak strain level by finite element analysis) (Pereira et al., 2015). Forty cycles were applied in each loading episode. 12-week old male cKO and WT mice (n>3/genotype) were loaded 3 times per week for 2 weeks and left and right tibia dissected 3 days after the final loading episode.

Whole mount staining

Male mice were euthanized by CO_2 and incubated for 24 hours in tap water. Carcasses were then scalded in hot tap water to enable removal of the skin, skinned and eviscerated, and then fixed in 95% ethanol for 3-5 days. The preparations were then incubated in 0.015% Alcian blue (pH 0.75) for 24 hours to stain sulphated glycosaminoglycans in the cartilage, rinsed twice in 95% ethanol and fixed in 95%

ethanol for another 2 days. Mice were then cleared of the remaining muscle by a 6 hour incubation in 1% KOH (w/v) and the bone was stained with fresh 0.005% Alizarin Red for 3 hours. Mice were then further cleared in 2% KOH (w/v) for 48 hours followed by decreasing concentrations of 2% KOH (w/v) in glycerol for 24 h each (80:20, 60:40, 40:60 and 20:80, respectively). The skeletal preparations were stored in 20:80 2% KOH:glycerol at room temperature.

Tissue processing for histological techniques

Soft tissues (liver, spleen, lung, heart and kidney) and tibia/femurs were dissected from freshly killed male and female mice and fixed in 4% paraformaldehyde (PFA) for 24 hours at 4ºC. Tibiae were subsequently decalcified in 10% ethylenediaminetetracetic acid (EDTA/PBS, pH 7.4 at 4ºC; Sigma Aldrich, Dorset, UK) for 3-4 weeks with regular changes. Soft tissues and legs were dehydrated and processed to paraffin wax using standard procedures. Sections (5µm) were cut and used for histological and immunohistochemical analysis. To analyse osteoclast and osteoblast numbers, sections were reacted for tartrate-resistant acid phosphatase activity (TRAP) and stained by H&E respectively, as described previously (Erlebacher et al., 1996). Osteoclasts were quantified per mm^2 of trabecular bone, and osteoblasts per mm of bone surface, in an identical region at an equivalent distance beneath the growth plate in all samples.

Immunohistochemistry

For immunohistochemical analysis, sections were dewaxed in xylene and rehydrated. Sections were incubated at 37 °C for 30 min in 1mg/ml trypsin for antigen demasking. Endogenous peroxidases were blocked by treatment with 3% H_2O_2 in methanol (Sigma). Ppdn antibodies (Polyclonal raised in Goat IgG; R&D systems) were used at a dilution of 1/100; and sclerostin antibodies (Polyclonal raised in Goat IgG; R&D systems) at a dilution of 1:200 with appropriate IgG controls. The Vectastain ABC universal kit (Vector Laboratories, Peterborough, UK) was used according to the manufacturer's instructions. The sections were dehydrated, counterstained with haematoxylin and mounted in DePeX.

Phalloidin staining

Femurs from male mice were decalcified as described above and then cryoprotected in 30% sucrose (w/v) at 4ºC for 48 hours. The femora were cut in the mediolateral

plane in serial longitudinal 20µm thick-sections using a cryostat and thaw-mounted on gelatin-coated slides for processing. Slides were dried at room temperature for 45 minutes, washed in PBS twice for 5 min each, and incubated with 0.1% Triton-X 100 (Sigma Aldrich) for 30 minutes and then rinsed with PBS. Slides were then incubated with Alexa Fluor 488-conjugated phalloidin (1:20; Life Technologies, Grand Island, NY) for 1 hour. Bone sections were washed in PBS and mounted in VectaShield (Vector Laboratories). Preparations were allowed to dry at room temperature for 12 hours.

Analysis of phalloidin staining

Sections were imaged on a Zeiss LSM 710 Laser Scanning Confocal Microscope with 488nm laser excitation and detection settings from 493 to 634nm. Z-stacks were produced with optimal Nyquist overlap settings using a 63x/1.4na oil immersion lens. Voxel sizes were 0.1x0.1x1.00µm in x,y,z planes respectively. A comparable region of interest was analysed for osteocyte parameters in all samples located in the diaphyseal cortical bone. Image stacks were imported into Bitplane Imaris 8.2.0 software and algorithms were created with Imaris FilamentTracer to render and measure dendritic processes. Surface rendering was used for osteocyte cell body measurements.

Micro-computed tomography (µCT) scanning

Tibiae from male and female mice were dissected and frozen at -20ºC until required. Scans were performed with an 1172 X-Ray Microtomograph (Skyscan, Belgium) to evaluate bone geometry. High-resolution scans with an isotropic voxel size of 5 µm were acquired (50 kV, 200µA, 0.5 mm aluminium filter, 0.6° rotation angle, 2 frame averaging, exposure time 1650). The projection images were reconstructed using NRecon software version 1.6.9.4 (Skyscan, Belgium) to produce tomograms that underwent processing during reconstruction to correct for beam-hardening and ring artefacts.

Morphometrical analysis

a. Trabecular bone

For the trabecular analysis, the base of the growth plate was used as a standard reference point. Trabecular bone was analysed in a 1mm region of the proximal tibia

250 µm from this reference point (towards the diaphysis). Data were analysed with CtAn software (Skyscan) as previously described (Staines et al., 2016b).

b. Whole bone cortical µCT analysis

Whole bone analysis was performed on datasets derived from whole CT scans using BoneJ (version 1.13.14) a plugin for ImageJ, as previously described (Javaheri et al., 2015). Following segmentation, alignment and removal of fibula from the dataset, a minimum bone threshold was selected using a histogram based method in ImageJ which utilises all pixels in a stack to construct a histogram and was further confirmed using ImageJ "threshold function". The grey level threshold ranged between 22000-22100 and was applied to all datasets to separate higher density bone from soft tissues and air. This threshold was used in "Slice Geometry" function within BoneJ to calculate bone cross sectional area (CSA), second moment of area around the minor axis (I_{min}), second moment of area around the major axis (I_{max}), mean cortical thickness determined by local thickness in two dimensions (Ct.Th), ellipticity and resistance to torsion (J). The most proximal and distal (10%) portions of the tibial length were excluded from analysis, as these regions include trabecular bone

Nano-computed tomography analysis

The samples were placed in Orthodontic Wax (Kerr, CA, USA) at 50 kV and 200 µA, 9800 ms exposure time with a 0.25 mm aluminium filter (99.999% purity, Goodfellow, Huntington, UK), voxel size of 0.6 µm, 360° at a rotation step of 0.25°. Two-frame averaging was used to improve the signal-to-noise ratio. We analysed 300 consecutive images from the tibia–fibula junction from each sample. Using the CtAn software, osteocyte lacunar indices were calculated by measuring the 3D parameters of each discreet object within the volume of interest after segmentation as described previously (Javaheri et al., 2015). Shape analysis of the lacunae was conducted utilizing 'Analyze Particles' function in BoneJ.

Mechanical testing

A Lloyd LRX5 materials testing machine (Lloyd Instruments, West Sussex, UK) fitted with a 100N load cell was used to determine bone stiffness and point of failure of tibiae. The span was fixed at 10 mm, and the cross-head was lowered at 1 mm/min. Data were recorded after every 0.2 mm change in deflection. Each bone was tested to failure, with failure points being identified as the point of maximum load from the

load–extension curve. The maximum stiffness was defined as the maximum gradient of the rising portion of this curve (Huesa et al., 2011).

RNA extraction and quantitative real-time PCR (RT-qPCR)

Total RNA was extracted using the RNEasy mini kit (Qiagen) according to the manufacturer's instructions. RNA samples were reverse-transcribed into cDNA using Superscipt II reverse transcriptase (Invitrogen). RT-qPCR was carried out in a Stratagene Mx3000P cycler with each reaction containing 50ng template DNA, 250nM forward and reverse primers (Primer Design, Southampton UK) (Sost: F – TGAGAACAACCAGACCATGAAC, R – TCAGGAAGCGGGTGTAGTG; Dmp1: F – ATACCACAATACTGAATCTGAAAGC, R – CACTATTTGCCTGTCCCTCTG; Phex: F – CTAACCACCCACTCCCACTT, R – CCAATAGACTCCAAACCTGAAGA; Atp5b: sequences not available) and PrecisionPlus Mastermix (Primer Design). The Ct values for the samples were normalised to that of Gapdh and the relative expression was calculated using the ΔΔCt method (Livak and Schmittgen, 2001). The amplification efficiencies of all the primers were between 90–100%.

Western blotting

Femurs from male mice had their epiphyses removed and were flushed to remove bone marrow, snap frozen and lysed in RIPA buffer (Sigma), containing protease inhibitors (Roche). Protein content was determined using the DC protein assay (Bio-Rad Laboratories). The lysates were run on 10% Bis–Tris gels. Following transfer, nitrocellulose films were blocked in 5% milk, and probed overnight at 4^{o}C with Pdpn primary antibody (R&D systems; 1:1000). The nitrocellulose was subsequently incubated with peroxidase labelled rabbit anti-goat antibodies (Dako) for a further 90min. ECL detection reagents were used to visualise bands on hyperfilm (GE Healthcare, Bucks, UK). Where necessary, the nitrocellulose was stripped using Restore Plus Stripping Buffer (GE Healthcare). Densitometry of western blotting was measured on three independent samples using Image J.

Serum phosphate analysis

Immediately before termination, blood was collected and incubated on ice for 30 minutes, before centrifugation at 15,000g for 10 minutes. The serum supernatant was

stored at -80°C until analysed for phosphate levels using a colorimetric Phosphate Assay Kit (Abcam; 1:100) according to the manufacturer's instructions.

Statistical analysis

Data are expressed as the mean ± S.E.M of at least 3 replicates per experiment. Results were analysed blinded. For cortical bone, graphs were developed using the R programming language "R", version 3.1.3 (R Foundation for Statistical Computing, Vienna, Austria; http://www.r-project.org). Normality and homogeneity of variance of all the data were checked using the Shapiro-Wilk and the Bartlett's test in R 3.1.3 respectively. Two-sample Student's-test was used to compare means between female cKO and fl/fl, and between male cKO and fl/fl. Kruskal-Wallis test was employed if either the normality or the homogeneity of variance assumptions were violated ($p \geq 0.05$). $P<0.05$ was considered to be significant and noted as *; P values of <0.01 and <0.001 were noted as '**' and '***' respectively.

Acknowledgements

We are grateful to the Arthritis Research UK for funding this research (20413 and 20581) and Elaine Seawright for her assistance with the experiments detailed. We are also extremely thankful to the BRF staff at the Roslin Institute, especially Gordon Melville. We are also grateful to the Biotechnology and Biological Sciences Research Council (BBSRC) for Institute Strategic Programme Grant Funding BB/J004316/1

Author Contributions

KAS, BJ, DJB, AAP & CF conceived and designed experiments and wrote the manuscript; PH conceived and designed experiments; MH, EI, EU & RF performed experiments and analysed data. All authors read, discussed and edited the manuscript.

Competing financial interests

All authors have no conflicts of interest with regards to competing financial interests

References

Balemans, W, Ebeling M, Patel N, Van Hul E, Olson P, Dioszegi M, Lacza C, Wuyts W, Van Den Ende J, Willems P, Paes-Alves AF, Hill S, Bueno M, Ramos FJ, Tacconi P, Dikkers FG, Stratakis C, Lindpaintner K, Vickery B, Foernzler D, Van Hul W. 2001. Increased bone density in sclerosteosis is due to the deficiency of a novel secreted protein (SOST). Human molecular genetics **10**, 537-543.

Cao YX, Ramirez MI, & Williams, MC. 2003. Enhanced binding of Sp1/Sp3 transcription factors mediates the hyperoxia-induced increased expression of the lung type I cell gene T1alpha. Journal of cellular biochemistry **89**, 887-901.

Dallas SL., Prideaux M, & Bonewald LF. 2013. The osteocyte: an endocrine cell ... and more. Endocrine reviews **34**, 658-690

De Souza RL, Matsuura M, Eckstein F, Rawlinson SC, Lanyon LE, Pitsillides AA. 2005. Non-invasive axial loading of mouse tibiae increases cortical bone formation and modifies trabecular organization: a new model to study cortical and cancellous compartments in a single loaded element. Bone **37**, 810-818.

Dobbs LG, Williams MC, & Gonzalez R. 1988 Monoclonal antibodies specific to apical surfaces of rat alveolar type I cells bind to surfaces of cultured, but not freshly isolated, type II cells. Biochimica et biophysica acta **970**, 146-156.

Groger M, Loewe R, Holnthoner W, Embacher R, Pillinger M, Herron GS, Wolff K, Petzelbauer P. 2004. IL-3 induces expression of lymphatic markers Prox-1 and podoplanin in human endothelial cells. Journal of immunology **173**, 7161-7169.

Hamers FP, Lankhorst AJ, van Laar TJ, Veldhuis WB, Gispen WH. 2001. Automated quantitative gait analysis during overground locomotion in the rat: its application to spinal cord contusion and transection injuries. Journal of neurotrauma **18**, 187-201.

Holmbeck K, Bianco P, Pidoux I, Inoue S, Billinghurst RC, Wu W, Chrysovergis K, Yamada S, Birkedal-Hansen H, Poole AR. 2005. The metalloproteinase MT1-MMP is required for normal development and maintenance of osteocyte processes in bone. Journal of cell science **118**, 147-156.

Hong YK, Harvey N, Noh YH, Schacht V, Hirakawa S, Detmar M, Oliver G. 2002. Prox1 is a master control gene in the program specifying lymphatic endothelial cell fate. Developmental dynamics : an official publication of the American Association of Anatomists **225**, 351-357.

Huesa C, Yadav MC, Finnilä MA, Goodyear SR, Robins SP, Tanner KE, Aspden RM, Millán JL, Farquharson C. 2011. PHOSPHO1 is essential for mechanically competent mineralization and the avoidance of spontaneous fractures. Bone 4**8**, 1066-1074.

Jain A, Karadag A, Fohr B, Fisher LW, Fedarko NS. 2002. Three SIBLINGs (small integrin-binding ligand, N-linked glycoproteins) enhance factor H's cofactor activity enabling MCP-like cellular evasion of complement-mediated attack. The Journal of biological chemistry **277**, 13700-13708.

Javaheri, B., Carriero A, Staines KA, Chang YM, Houston DA, Oldknow KJ, Millan JL, Kazeruni BN, Salmon P, Shefelbine S, Farquharson C, Pitsillides AA. 2015. Phospho1 deficiency transiently modifies bone architecture yet produces consistent modification in osteocyte differentiation and vascular porosity with ageing. Bone **81**, 277-291.

Liu F, Woitge HW, Braut A, Kronenberg MS, Lichtler AC, Mina M, Kream BE. 2004. Expression and activity of osteoblast-targeted Cre recombinase transgenes in murine skeletal tissues. The International journal of developmental biology **48**, 645-653.

Livak KJ, Schmittgen TD. 2001. Analysis of relative gene expression data using real-time quantitative PCR and the 2(-Delta Delta C(T)) method. Methods **25**:402–408.

Lu Y, Yuan B, Qin C, Cao Z, Xie Y, Dallas SL, McKee MD, Drezner MK, Bonewald LF, Feng JQ. 2011. The biological function of DMP-1 in osteocyte maturation is mediated by its 57-kDa C-terminal fragment. J Bone Miner Res **26**, 331-340.

Martín-Villar E, Megías D, Castel S, Yurrita MM, Vilaró S, Quintanilla M. 2006. Podoplanin binds ERM proteins to activate RhoA and promote epithelial-mesenchymal transition. Journal of cell science **119**, 4541-4553.

Martín-Villar E, Borda-d'Agua B, Carrasco-Ramirez P, Renart J, Parsons M, Quintanilla M, Jones GE. 2014. Podoplanin mediates ECM degradation by squamous carcinoma cells through control of invadopodia stability. Oncogene **34**, 4531-4544.

Masocha W, Parvathy SS. 2009. Assessment of weight bearing changes and pharmacological antinociception in mice with LPS-induced monoarthritis using the Catwalk gait analysis system. Life Sci. **85**, 462-469.

Nakashima T, Takayanagi H. 2011. New regulation mechanisms of osteoclast differentiation. Annals of the New York Academy of Sciences **1240**, E13-18.

Nefussi JR, Sautier JM, Nicolas V, Forest N. 1991. How osteoblasts become osteocytes: a decreasing matrix forming process. Journal de biologie buccale **19**, 75-82.

Palumbo C, Ferretti M, Marotti G. 2004. Osteocyte dendrogenesis in static and dynamic bone formation: an ultrastructural study. The anatomical record. Part A, Discoveries in molecular, cellular, and evolutionary biology **278**, 474-480.

Pereira AF, Javaheri B, Pitsillides AA, Shefelbine, SJ. 2015. Predicting cortical bone adaptation to axial loading in the mouse tibia. Journal of the Royal Society, Interface / the Royal Society **12**, 0590.

Ramirez MI, Millien G, Hinds A, Cao Y, Seldin DC, Williams MC. 2003. T1alpha, a lung type I cell differentiation gene, is required for normal lung cell proliferation and alveolus formation at birth. Developmental biology **256**, 61-72.

Rishi AK, Joyce-Brady M, Fisher J, Dobbs LG, Floros J, VanderSpek J, Brody JS, Williams MC. 1995. Cloning, characterization, and development expression of a rat lung alveolar type I cell gene in embryonic endodermal and neural derivatives. Developmental biology **167**, 294-306.

Rodda SJ, McMahon AP. 2006. Distinct roles for Hedgehog and canonical Wnt signaling in specification, differentiation and maintenance of osteoblast progenitors. Development **133**, 3231-3244.

Saffar KP, Jamilpour N, Rajaai SM. 2009. How does the bone shaft geometry affect its Bending Properties? Am. J. Appl. Sci. **6**(3): 463-470.

Schacht V, Ramirez MI, Hong YK, Hirakawa S, Feng D, Harvey N, Williams M, Dvorak AM, Dvorak HF, Oliver G, Detmar M. 2003. T1alpha/podoplanin deficiency disrupts normal lymphatic vasculature formation and causes lymphedema. EMBO J. **22**, 3546-3556.

Scholl FG, Gamallo C, Vilaro S, Quintanilla M. 1999. Identification of PA2.26 antigen as a novel cell-surface mucin-type glycoprotein that induces plasma membrane extensions and increased motility in keratinocytes. Journal of cell science **112** (Pt 24), 4601-4613.

Skerry TM, Bitensky L, Chayen J, Lanyon LE. 1989. Early strain-related changes in enzyme activity in osteocytes following bone loading in vivo. J Bone Miner Res **4**, 783-788.

Sprague L, Wetterwald A, Heinzman U, Atkinson MJ. 1996. Phenotypic changes following over-expression of sense or antisense E11 cDNA in ROS 17/2.8 cells. J Bone Miner Res **11**, 151-151.

Staines KA, Macrae VE, Farquharson C. 2012. The importance of the SIBLING family of proteins on skeletal mineralisation and bone remodelling. The Journal of endocrinology **214**, 241-255.

Staines KA, Zhu D, Farquharson C, Macrae VE. 2013. Identification of novel regulators of osteoblast matrix mineralization by time series transcriptional profiling. J Bone Mineral Metab. **32**:240–251.

Staines KA, Prideaux M, Allen S, Buttle DJ, Pitsillides AA, Farquharson C. 2016a. E11/Podoplanin Protein Stabilization Through Inhibition of the Proteasome Promotes Osteocyte Differentiation in Murine in Vitro Models. J. Cell. Physiol. **231**, 1392-1404.

Staines KA, Madi K, Mirczuk SM, Parker S, Burleigh A, Poulet B, Hopkinson M, Bodey AJ, Fowkes RC, Farquharson C, Lee PD, Pitsillides AA. 2016b. Endochondral Growth Defect and Deployment of Transient Chondrocyte Behaviors Underlie Osteoarthritis Onset in a Natural Murine Model. Arthritis & rheumatology **68**, 880-891.

Suzuki H, Amizuka N, Oda K, Li M, Yoshie H, Ohshima H, Noda M, Maeda T. 2005. Histological evidence of the altered distribution of osteocytes and bone matrix synthesis in klotho-deficient mice. Archives of histology and cytology **68**, 371-381.

Takai Y, Sasaki T, Matozaki T. 2001. Small GTP-binding proteins. Physiol. Rev. **81**, 153-208.

Xiao Z, Zhang S, Cao L, Qiu N, David V, Quarles LD. 2010. Conditional disruption of Pkd1 in osteoblasts results in osteopenia due to direct impairment of bone formation. The Journal of biological chemistry **285**, 1177-1187.

Xiong J, Onal M, Jilka RL, Weinstein RS, Manolagas SC, O'Brien CA. 2011 Matrix-embedded cells control osteoclast formation. Nat. Med. **17,** 1235-1241.

Ye L, MacDougall M, Zhang S, Xie Y, Zhang J, Li Z, Lu Y, Mishina Y, Feng JQ. 2004. Deletion of dentin matrix protein-1 leads to a partial failure of maturation of predentin into dentin, hypomineralization, and expanded cavities of pulp and root canal during postnatal tooth development. The Journal of biological chemistry **279**, 19141-19148.

Ye L, Mishina Y, Chen D, Huang H, Dallas SL, Dallas MR, Sivakumar P, Kunieda T, Tsutsui TW, Boskey A, Bonewald LF, Feng JQ. 2005. Dmp1-deficient mice display severe defects in cartilage formation responsible for a chondrodysplasia-like phenotype. The Journal of biological chemistry **280**, 6197-6203.

Zhang M, Xuan S, Bouxsein ML, von Stechow D, Akeno N, Faugere MC, Malluche H, Zhao G, Rosen CJ, Efstratiadis A, Clemens TL. 2002. Osteoblast-specific knockout of the insulin-like growth factor (IGF) receptor gene reveals an essential role of IGF signaling in bone matrix mineralization. The Journal of biological chemistry **277**, 44005-44012.

Zhang K, Barragan-Adjemian C, Ye L, Kotha S, Dallas M, Lu Y, Zhao S, Harris M, Harris SE, Feng JQ, Bonewald LF.2006. E11/gp38 selective expression in osteocytes: regulation by mechanical strain and role in dendrite elongation. Mol. Cell. Biol. **26**, 4539-4552.

Figure Legends

Figure 1. (A) Schematic of the Pdpn floxed allele before and after deletion of the loxP cassette containing exon 3 via osteocalcin cre (Oc-cre) mediated recombination. **(B)** PCR analysis of genomic DNA from the long bones of fl/fl, and cKO mice with primers for the Tm1c allele (before cre recombination), and the Tm1d allele (~440bp, after cre recombination). **(C)** Immunohistochemical labelling of Pdpn in the lung, kidney, spleen, heart, liver, muscle, and growth plate, of 6-week old mice. Images are representative of n=4/sex/genotype. Scale bar = 20µm. **(D)** Immunohistochemical labelling of Pdpn in the trabecular bone and cortical bone of 6-week old mice. Arrows are pointing at embedded osteocytes within the trabecular and cortical bone and their dendritic processes projecting from the cell bodies. Images are representative of n=4/sex/genotype. Scale bar = 20µm. **(E)** Quantification of osteocytes positive for Pdpn immunolabelling relative to negatively labelled osteocytes (n=3/genotype) P<0.001*** **(F)** Western blotting for Pdpn (~37kDa) in cortical bone protein lysates from 6-week old mice. β-actin was used as a loading control. Whole mount Alcian Blue and Alizarin Red stained skeletal preparations of 6- week old male **(G)** fl/fl, and **(H)** cKO mice (scale bar = 10mm) including hindlimb and calvaria preparations (scale bar = 5mm).

Figure 2. Whole bone analyses of cortical bone between 10–90% of total tibial length, excluding proximal and distal metaphyseal bone, of female fl/fl (brown), female cKO (orange), male fl/fl (black) and male cKO (grey) tibia at 6 weeks of age showing **(A)** cross sectional area (CSA; mm^2) **(B)** mean cross sectional thickness (mm). Graphs represent mean ± S.E.M, n=4/group. P<0.05 was considered to be significant and P values of p≤0.01-0.05 were noted as green, p≤0.001-0.01 as yellow, and p≤0.000-0.001 as red. Not significant is noted as blue.

Figure 3. Whole bone analyses of cortical bone between 10–90% of total tibial length, excluding proximal and distal metaphyseal bone, of female fl/fl (brown), female cKO (orange), male fl/fl (black) and male cKO (grey) tibia at 6 weeks of age showing **(A)** I_{min} (mm^4) **(B)** I_{max} (mm^4) **(C)** ellipticity **(D)** resistance to torsion **(**J; mm^4) Graphs represent mean ± S.E.M, n=4/group. P<0.05 was considered to be significant and P values of p≤0.01-0.05 were noted as green, p≤0.001-0.01 as yellow, and p≤0.000-0.001 as red. Not significant is noted as blue.

Figure 4. (A) Alizarin red staining of primary osteoblast cultures from Pdpn cKO and fl/fl mice over a 21 day culture period. (B) Quantification of Alizarin red staining. RT-qPCR analysis of osteocyte marker genes **(C)** Sost **(D)** Phex **(E)** Dmp1 in mineralizing primary osteoblast cultures from Pdpn cKO and fl/fl mice over a 21 day culture period. **(F)** Immunohistochemical labeling of sclerostin in the cortical bone of 6-week old mice. Arrows are pointing at embedded osteocytes within the cortical bone and their dendritic processes projecting from the cell bodies. Images are representative of n=4/sex/genotype. Scale bar = 20µm. **(G)** Osteoclast cell numbers (OC.N/mm^2) in the trabecular bone of 6-week old cKO and fl/fl mice (n=4/genotype) **(H)** Osteoblast cell numbers (OB.N/mm bone surface (BS)) in the trabecular bone of 6-week old cKO and fl/fl mice (n=4/genotype) **(I)** Serum phosphate levels in cKO and fl/fl mice (n=6/genotype). Data are represented as mean ± S.E.M. P<0.05*, P<0.01**, P<0.001***.

Figure 5. Representative images of fl/fl and cKO mice in **(A)** control **(B)** loaded limbs. **(C)** Cortical cross-sectional thickness at 37% of the tibia length as assessed by microCT analysis. **(D)** Immunohistochemical labeling of sclerostin in osteocytes of cortical bone of loaded and control 6-week old Pdpn cKO and fl/fl mice. . Arrows are pointing at embedded osteocytes within the cortical bone and their dendritic processes projecting from the cell bodies. Images are representative of n=4/sex/genotype. Scale bar = 20µm. **(E)** Laser confocal z-stack, single channel outlining phalloidin-Factin staining was imaged in the cortical bone. Imaris cell surface rendering was applied to cell bodies and Imaris FilamentTracer applied to dendritic processes and these were coloured according to length. Quantification of osteocyte parameters in 6-week old male fl/fl, and cKO **(F)** Total number of complete cell bodies in 3 volume fields. **(G)** Cell body volume (µm^3) **(H)** Cell body sphericity **(I)** Total number of dendrites in 3 volume fields **(J)** Dendrite volume (µm^3) **(K)** Dendrite length (µm). Data are represented as mean ± S.E.M. P<0.05*, P<0.01**, P<0.001***.

Table 1: Trabecular parameters from microCT analysis of 6-week old male and female fl/fl, and cKO mice (n=4/genotype/sex). [a] P<0.05* in comparison to male equivalent genotype. Data are represented as mean ± S.E.M.

Sex		BV/TV (%)	Tb.N (μm^{-1})	Tb.Th (μm)	Tb.Sp (μm)	Tb.Pf (μm^{-1})
M	**fl/fl**	0.40 ± 0.05	1.14 ± 0.06	28.1 ± 3.53	1.19 ± 0.06	9.84 ± 3.71
	cKO	0.38 ± 0.03	1.12 ± 0.07	30.3 ± 1.57	1.11 ± 0.09	10.6 ± 3.12
F	**fl/fl**	0.23 ± 0.03[a]	1.19 ± 0.02	32.7 ± 1.65	0.96 ± 0.08	5.96 ± 3.05
	cKO	0.23 ± 0.03	1.07 ± 0.03	33.2 ± 3.36	1.12 ± 0.08	9.54 ± 2.68

Table 2: 3 point bending analysis of 6-week old male and female fl/fl, and cKO mice (n=4/genotype/sex). Data are represented as mean ± S.E.M. [a] P<0.05* in comparison to male equivalent genotype. [b] P<0.01** in comparison to female fl/fl. Data are represented as mean ± S.E.M.

Sex		Maximum load (N)	Deflection at Maximum Load (mm)	Work to Maximum Load (J)	Stiffness (N/m)	Load at Rupture (N)	Deflection at Rupture (mm)	Work to Rupture (J)
M	fl/fl	5.81 ± 0.65	0.60 ± 0.09	0.002 ± 0.00	17.7 ± 0.66	4.06 ± 0.45	0.80 ± 0.14	0.003 ± 0.00
	cKO	5.95 ± 0.26	0.78 ± 0.14	0.002 ± 0.00	16.4 ± 0.97	4.22 ± 0.19	1.08 ± 0.16	0.004 ± 0.00
F	fl/fl	4.58 ± 0.34	0.66 ± 0.04	0.002 ± 0.00	12.6 ± 1.42	3.21 ± 0.24[a]	0.90 ± 0.02	0.002 ± 0.00
	cKO	5.30 ± 0.51	0.68 ± 0.06	0.002 ± 0.00	19.1 ± 1.44[b]	3.88 ± 0.36	0.96 ± 0.11	0.003 ± 0.00

Table 3: Porosity parameters representing lacuna and vascular porosity of fl/fl and cKO mice detailing the effect of genotype. Data represent means ± SEM with group sizes of n = 4 for fl/fl and cKO mice.

Morphometric index	fl/fl n=4	cKO n=4	Effect of Genotype
Bone parameter			
Ct.TV (mm^{-3})	0.101 ± 0.017	0.078 ± 0.003	NS
Canal parameters			
N.Ca	52 ± 14.634	34 ± 12.124	NS
N.Ca/Ct.TV (mm^{-3})	530 ± 169.45	419 ± 134.24	NS
Ca.V/Ct.TV (%)	0.005 ± 0.001	0.003 ± 0.001	NS
Lacunae parameters			
N.Lc	1792 ± 353	1037 ± 383	NS
N.Lc/Ct.TV (mm^{-3})	18611 ± 4505	13083 ± 4497	NS
Lc.V/Ct.TV (%)	**0.004 ± 0.000**	**0.003 ± 0.000**	**NS**

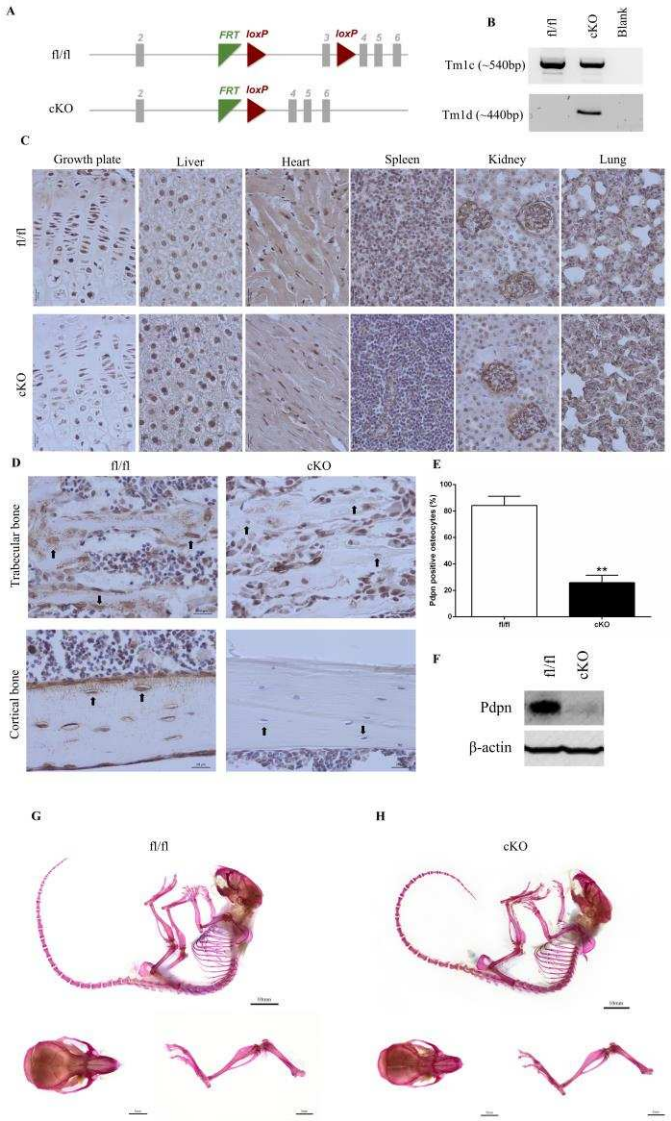

Figure 1

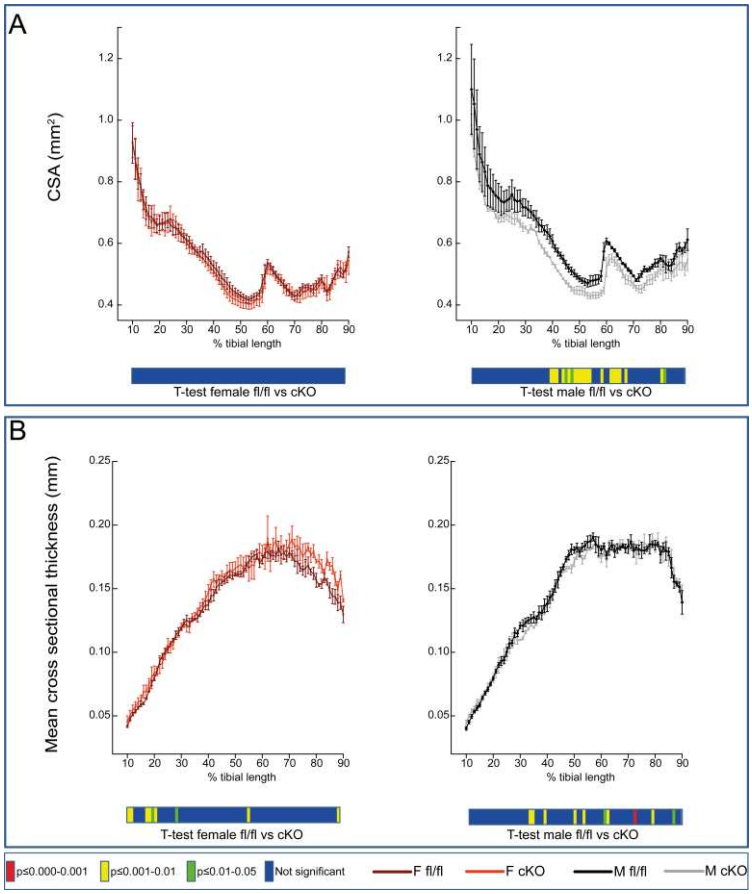

Figure 2

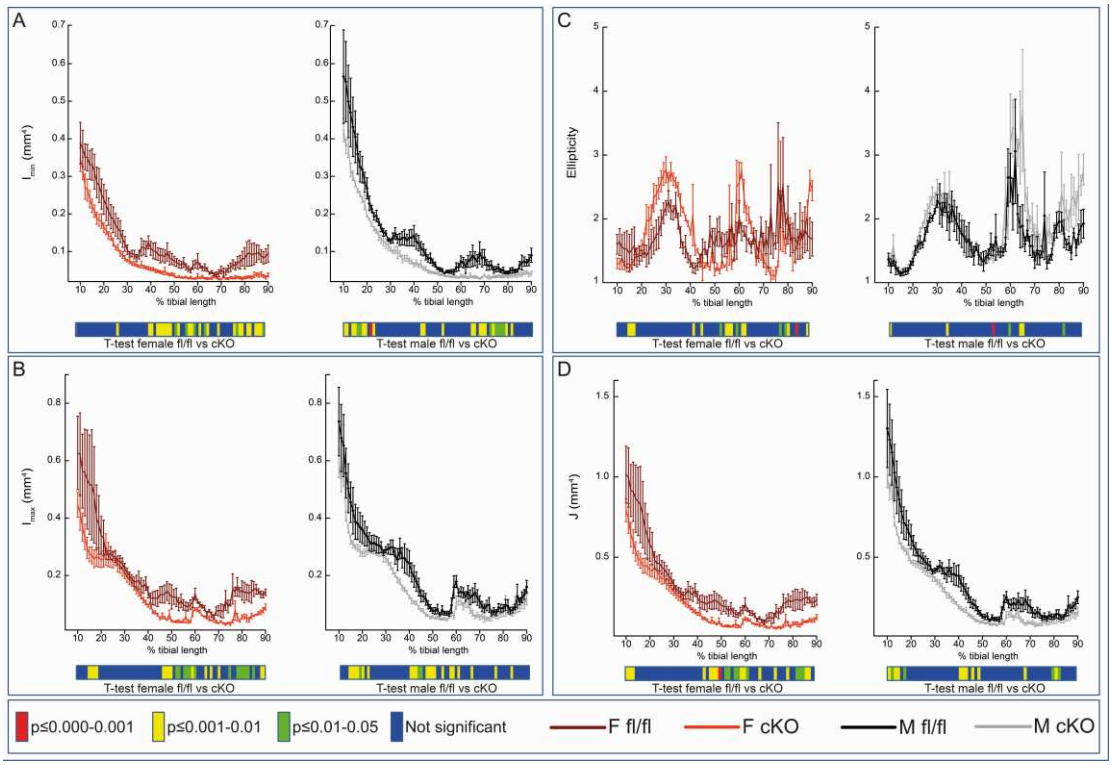

Figure 3

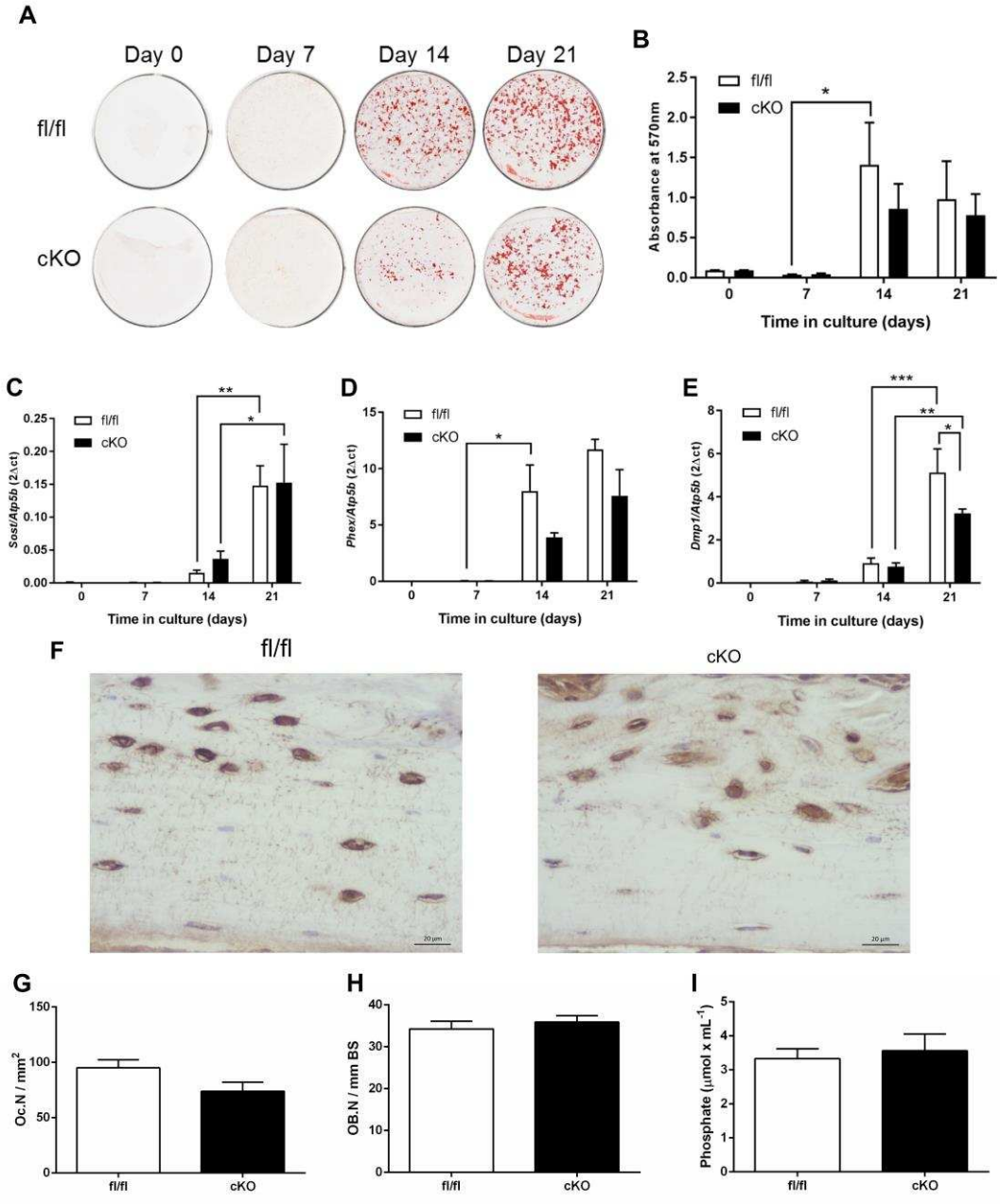

Figure 4

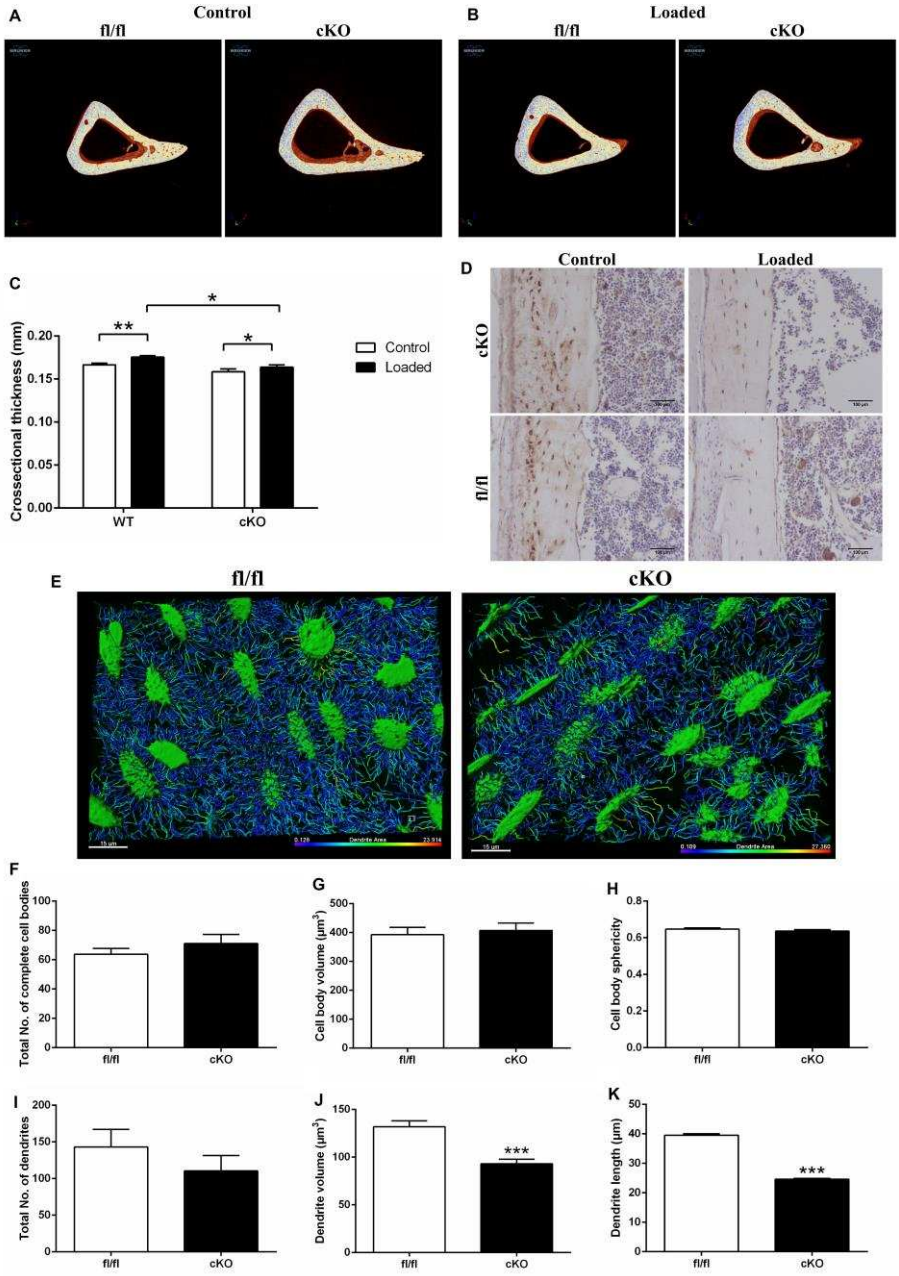

Figure 5